ORIGINAL PAPER

High temperature water electrolysis using metal supported solid oxide electrolyser cells (SOEC)

G. Schiller · A. Ansar · M. Lang · O. Patz

Abstract Metal supported cells as developed according to the DLR SOFC concept by applying plasma deposition technologies were investigated for use as solid oxide electrolyser cells (SOEC) for high temperature steam electrolysis. Cells consisting of a porous ferritic steel support, a diffusion barrier layer, a Ni/YSZ hydrogen electrode, a YSZ electrolyte and a LSCF oxygen electrode were electrochemically characterised by means of i-V characteristics and electrochemical impedance spectroscopy measurements including a long-term test over 2000 h. The cell voltage during electrolysis operation at a current density of -1.0 A cm^{-2} was 1.28 V at an operating temperature of 850 °C and 1.4 V at 800 °C. A long-term test run over 2000 h with a steam content of 43% at 800 °C and a current density of -0.3 A cm^{-2} showed a degradation rate of 3.2% per 1000 h. The impedance spectra revealed a significantly enhanced polarisation resistance during electrolysis operation compared to fuel cell operation which was mainly attributed to the hydrogen electrode.

1 Introduction

The use of renewable energy has attained increasing interest over the past years. For a wider utilisation of

G. Schiller (✉) · A. Ansar · M. Lang · O. Patz
Deutsches Zentrum für Luft- und Raumfahrt (DLR), Institut für Technische Thermodynamik, Pfaffenwaldring 38-40, D-70569 Stuttgart, Germany
e-mail: guenter.schiller@dlr.de

renewable energy sources such as wind, photovoltaic, solar thermal power and others chemical energy carriers are needed for electricity storage to maintain the high delivery stability in the energy infrastructure. Electrolysis technologies are highly suited for the production of hydrogen based energy carriers. In the low temperature range below 100 °C alkaline water electrolysers are commercially available [1] and some development work has been performed in the last decades to further improve energy efficiency of the process [2, 3]. With conventional alkaline water electrolysers efficiencies of around 65% are reached whereas efficiencies exceeding 80% can be achieved by applying advanced technology with catalytically activated electrodes [4]. High temperature electrolysers which are operated in the temperature range of 700–1000 °C offer some additional advantages compared to the low temperature techniques. The higher operating temperature results in faster reaction kinetics thus enabling potentially high energy efficiency. From a thermodynamic point of view part of the energy demand for the endothermic water splitting reaction can be obtained from heat produced within the cell. The electric energy demand can be further significantly reduced if high temperature heat from renewable energy sources such as geothermal or solar thermal power, from nuclear power or waste heat from industrial processes is available. Furthermore, it is possible with high temperature electrolysis to not only split water steam but also carbon dioxide or a mixture of both to produce synthesis gas (syngas) or other energy carriers such as methane or methanol by subsequent catalytic conversion [5, 6].

Already during the 1980's the development of solid oxide electrolyser cells (SOEC) for high temperature steam electrolysis was reported by Dönitz et al. obtained within the "Hot Elly" project [7–10] and by Westinghouse [11]

Table 1 Characteristics of used metal supported cells

Functional layer	Reference	Composition	Thickness (μm)	Fabrication route
Substrate	Plansee IT11	Fe-26Cr (Mn, Mo, Ti, Y_2O_3)	950–1050	PM
Barrier Layer	HC Starck	$La_{0.6}Sr_{0.2}Ca_{0.2}CrO_3$	30–50	APS
H_2-electrode	Gen4	NiO-YSZ (1:1 mass)	40–60	APS
Electrolyte	Gen3	9.5 mol% YSZ	40–60	VPS
O_2-electrode	Gen3	LSM/LSCF	25–35	APS
		LSM/LSCF	15–40	Screen printed

Table 2 Plasma processing parameters for functional layers of SOEC

	Process	Vessel pressure (mbar)	Plasma torch type	Standoff distance (mm)	Plasma enthalpy nbsp;(MJ kg^{-1})
DBL	APS	Ambient	F4 V	90	11.2
H_2-electrode	APS	Ambient	F4-V21	82	14.5
Electrolyte	VPS	80	F4-M3-6 mm	280	15.9
O_2-electrode	APS	Ambient	F4-V21	85	9.8

on the basis of tubular cells but later stopped due to lower energy prices but also due to technical problems. In the past few years renewed interest on the SOEC technology appeared based on the progress achieved with planar SOFC technology [12–17]. The feasibility of planar SOFC cells and their limitations during electrolysis operation was investigated within the EU project Hi2H2 (Highly Efficient High Temperature Hydrogen Production by Water Electrolysis) [18]. Cells fabricated by wet ceramic processes and by plasma spray technology were tested and characterised by the European Institute for Energy Research (EIfER), Karlsruhe, Germany, Risø National Laboratory (Risø/DTU), Denmark [19–23], Swiss Federal Laboratories for Materials Testing and Research (EMPA), Switzerland, and German Aerospace Center (DLR), Germany. Recent results on metal supported cells (MSC) which have been fabricated by plasma spray technology at DLR Stuttgart and tested during fuel cell and electrolysis operation are presented.

2 Experimental details
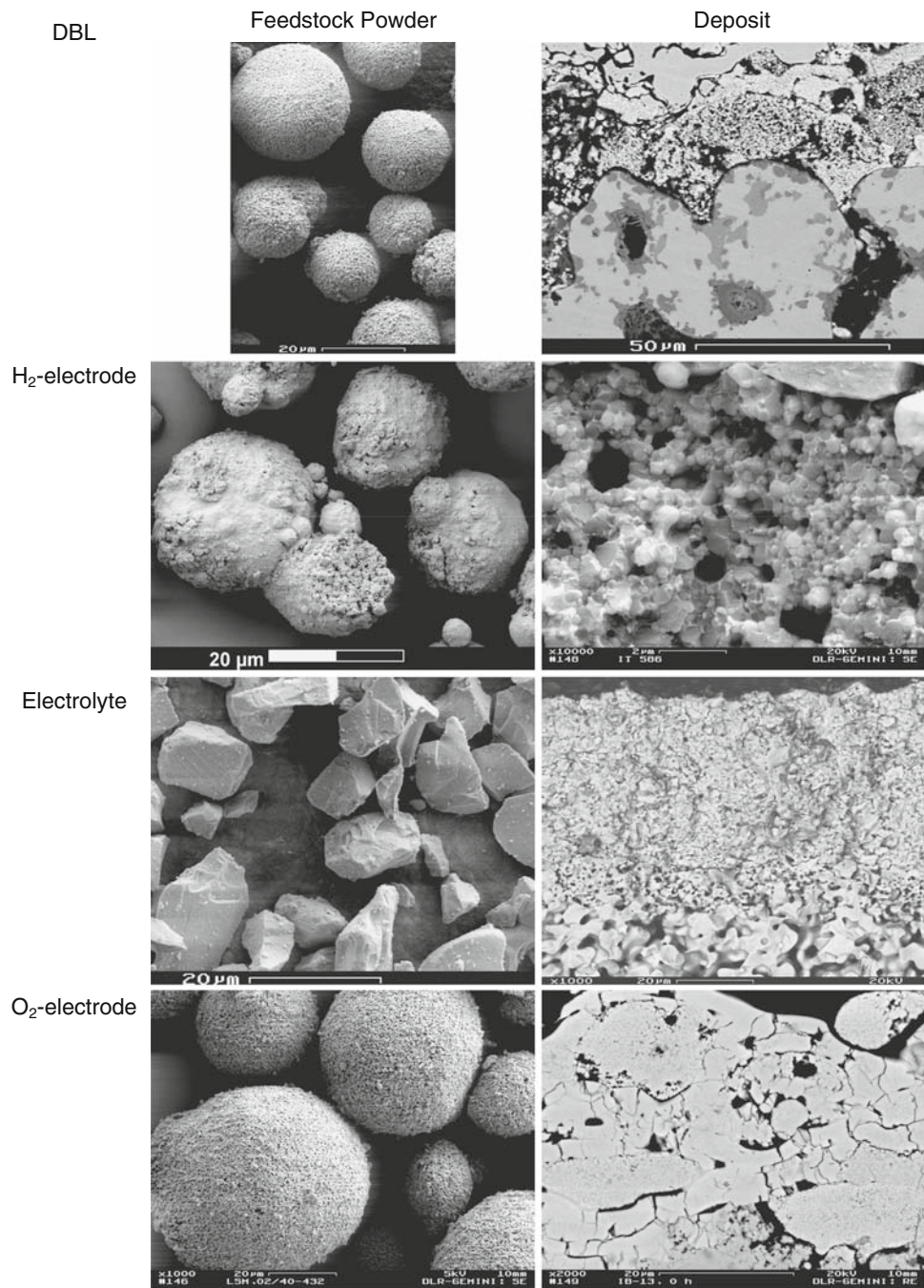
2.1 Manufacturing of SOEC

Metal supported cells developed at DLR by applying plasma deposition technologies were used as SOEC for high temperature steam electrolysis. The cells consisted of a 1 mm thick porous metal sheet of ferritic steel (IT11) from Plansee, Austria, which serves as a substrate support. On top of it a diffusion barrier layer (DBL) was deposited either by plasma spraying or PVD process. Such a highly porous ceramic DBL on the basis of doped perovskite-type

material has been developed at DLR to prevent mutual diffusion of Cr, Fe and Ni species from substrate to hydrogen electrode and vice versa [24–26]. A Ni/YSZ hydrogen electrode ($\sim$50 μm thick), a YSZ electrolyte ($\sim$40 μm thick) and a LSCF oxygen electrode ($\sim$30 μm thick) were subsequently deposited by plasma spray technology where atmospheric conditions (APS) were applied for the porous electrodes and reduced operating pressure (VPS) for the dense electrolyte layer. The characteristics of the MSC used are summarised in Table 1, Table 2 lists typical processing parameters for different deposits. The micrographs of feedstock powders and produced deposits for each functional layer are given in Fig. 1. Figure 2 shows an optical micrograph of a metallographic cross section of this cell type. More details on cell fabrication are given in [27–29].

2.2 Electrochemical characterisation

The cells with an active area of 12.5 cm^2 were tested in a SOFC test rig that was modified for electrolysis operation. This modification comprised the implementation of a humidification system and capacitive dew point sensors for monitoring of humidity, a battery test system from BaSyTec, Germany, as a switchable source/load and automatic refilling of the humidification unit for long-term tests. The circular cells were mounted into a ceramic cell housing and placed between the ceramic flow fields of the hydrogen and oxygen electrode. The current collection from the cell was accomplished by two coarse platinum meshes; one below the substrate and one above the O_2-electrode. Pt wires were welded to the meshes to provide connection to the external circuit. The hydrogen/steam gas feed and exhaust feed was

Fig. 1 Micrographs of feedstock materials and manufactured deposits of functional layers

achieved by two concentric ceramic tubes with an inner tube for H_2/H_2O and air gas supply, respectively, and exhaust removal through the annular gap between the two tubes. The sealing was done by gold rings and glass sealant paste. A cross sectional view of the set-up for cell characterisation is shown in Fig. 3. The cells were characterised in both fuel cell and electrolysis operation by i-V characteristics and electrochemical impedance spectroscopy measurements using a Zahner IM6 system. Long-term electrolysis tests were performed by monitoring the cell voltage as a function of time. The operating temperature was 800 °C for long-term tests and varied between 750 and 850 °C during i-V characterisation. The gas flow rates were 40 mL min^{-1} cm^{-2} H_2, 16 mL min^{-1} cm^{-2} H_2O (30% steam content) and 30 mL min^{-1} cm^{-2} H_2O (43% steam content), respectively, and 160 mL min^{-1} cm^{-2} air during electrolysis operation.

For the test runs with single repeating units (SRU) a metallic interconnect plate was used consisting of Cro-Fer22APU which contained channels for gas distribution and a plasma sprayed protective coating consisting of $MnCo_2O_4$. The circular cell and the coated interconnect

Fig. 2 Optical micrograph of a plasma sprayed SOFC cell

LaSrMnO$_3$-cathode

8YSZ-electrolyte

Ni/8YSZ-anode

La$_{0.7}$Sr$_{0.15}$Ca$_{0.15}$CrO$_3$-barrier layer

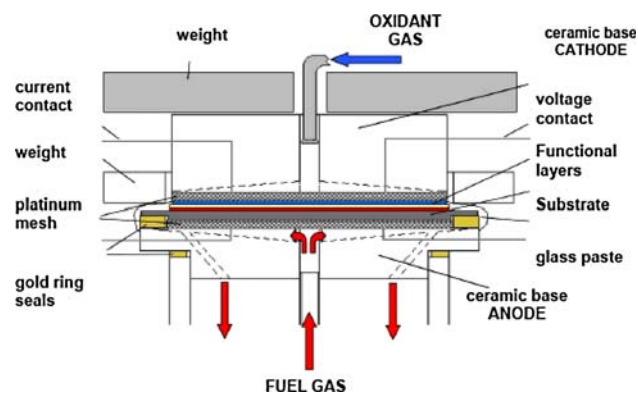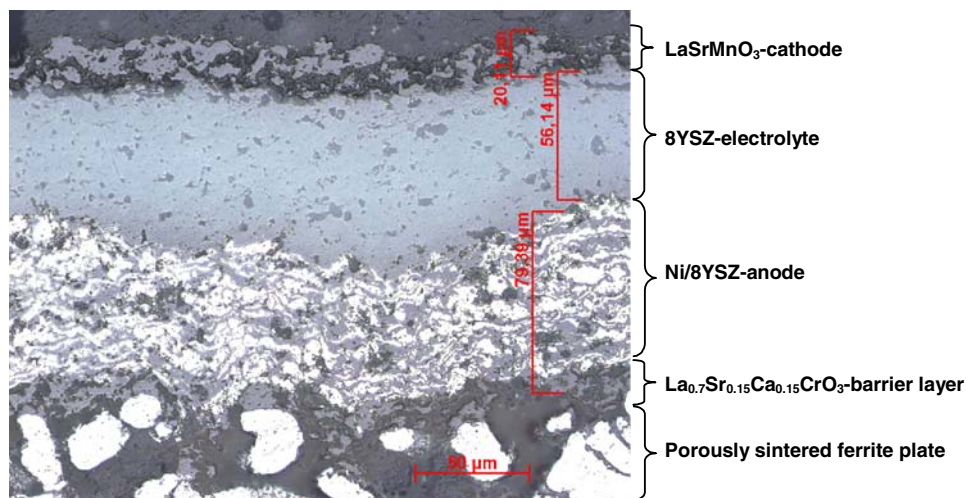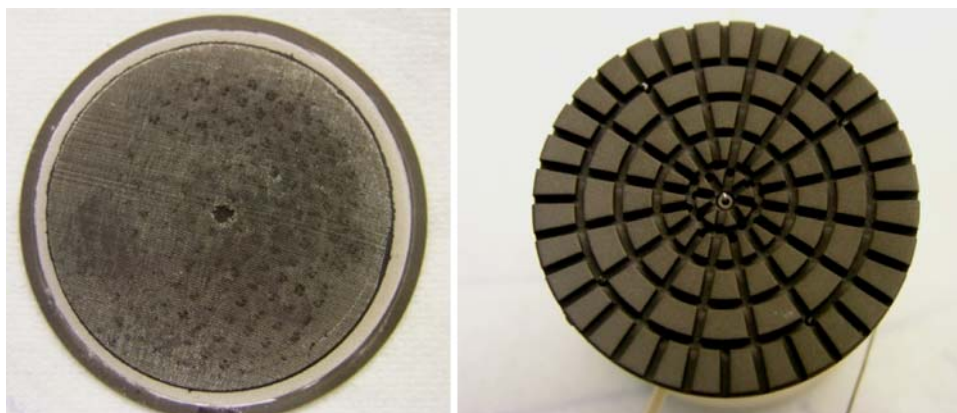Porously sintered ferrite plate

Fig. 3 Cross sectional view of the set-up for cell characterisation

plate used are depicted in Fig. 4. For contacting the cell with the interconnect a Pt grid in combination with a LSM contact paste was used that provided superior properties than using contact paste only. Probes for voltage measurement were placed at the interconnect and at the O$_2$-electrode which made it possible to determine the contact resistance.

3 Results and discussion

The cell performance of a single MSC cell in both fuel cell and electrolysis mode measured in the temperature range 750–850 °C is shown in Fig. 5. About 70% hydrogen and 30% steam was fed as inlet gas to the Ni/YSZ electrode. Positive current density refers to fuel cell operation and negative current density to electrolysis operation. At 800 °C the cell voltage at a current density of -1.0 A cm^{-2} was about 1.4 V and at 850 °C it was as low as 1.28 V. At moderate current density such as -0.3 A cm^{-2} as was applied as constant load during a long-term test run, the cell voltage was in the range of 1.07 V at 800 °C and 1.04 V at 850 °C. Variation of the steam content from 43% to 92% that has been performed with another cell revealed that the cell performance increases with higher steam content. This effect is strongly pronounced at a temperature of 800 °C and below but at 850 °C a higher steam content did not affect the cell performance significantly.

A long-term test run over a period of more than 2000 h with a constant current density of -0.3 A cm^{-2} at 800 °C

Fig. 4 Circular MSC cell and coated interconnect plate for testing of the single repeating unit

Fig. 5 I-V and i-p characteristics of a MSC cell during both fuel cell and electrolysis operation in the temperature range 750–850 °C and a gas flow of 40/16/ 160 mL min^{-1} cm^{-2} H$_2$/H$_2$O/ air (30% steam)
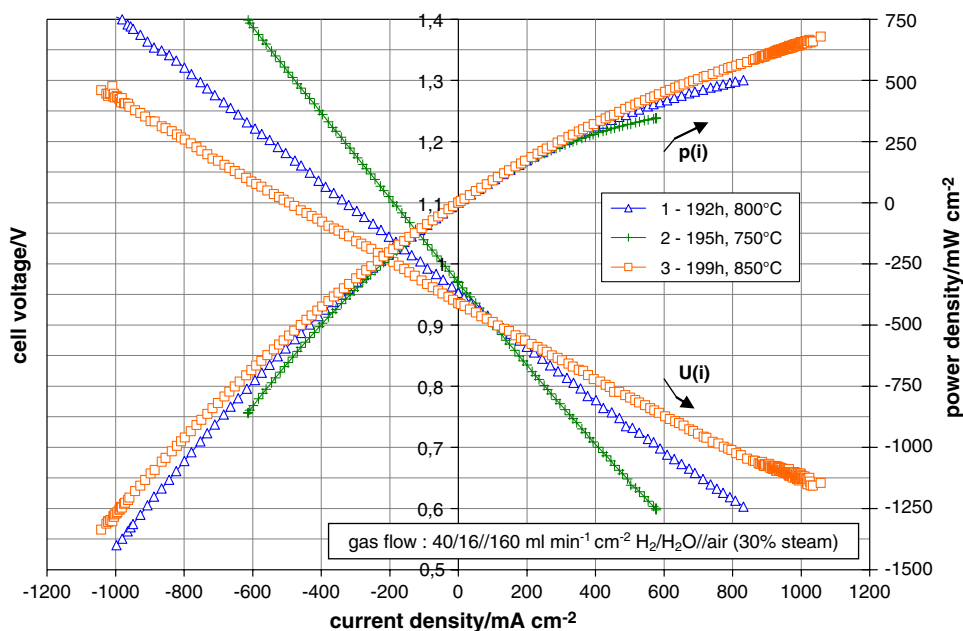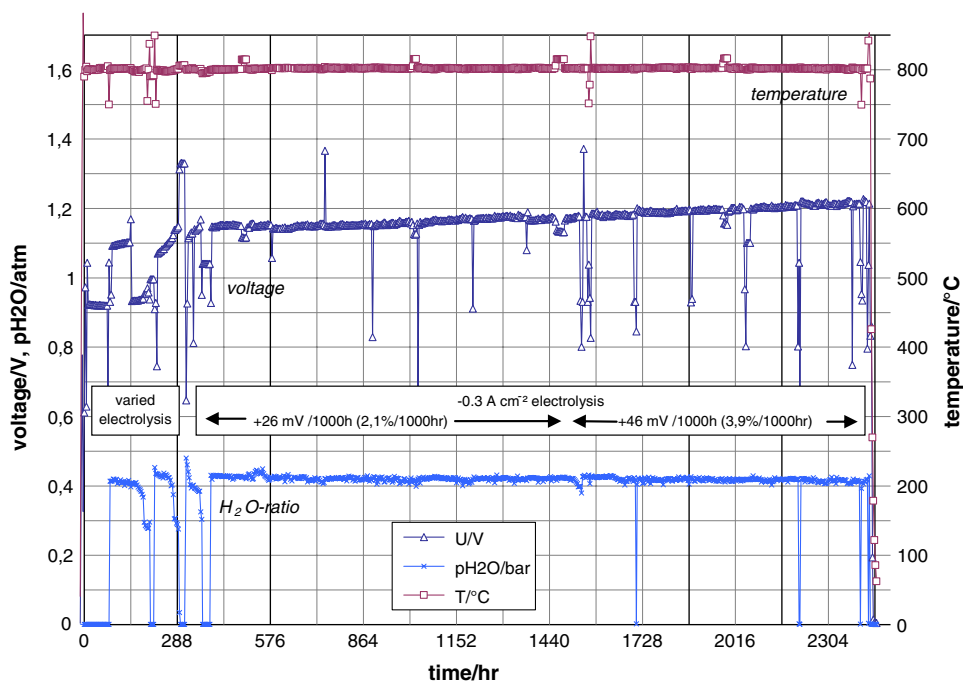
Fig. 6 Long-term test run of a MSC cell with a continuous load of −0.3 A cm^{-2} in electrolysis mode over more than 2000 h of operation; temperature (top), voltage (middle) and steam partial pressure (bottom) were monitored

was carried out starting after 394 h of operation. The steam content at the hydrogen electrode was kept constant at 43% for the whole test run. The cell voltage was monitored over time and i-V and impedance characterisation was performed every 150 h. The results of the durability test are summarised in Fig. 6. The cell voltage increased by about 26 mV during the first 1000 h of long term operation which corresponds to a degradation of 2.1% 1000 h^{-1}. During the next 1000 h (1400 h to 2400 h) an increase in cell voltage of 46 mV or 3.9% 1000 h^{-1}, respectively, was observed. This results in an increase of 72 mV for the whole period

of 2027 h corresponding to a degradation rate of 3.2% 1000 h^{-1}. These different values might be caused by different degradation mechanisms, e.g., changes in the microstructure of the electrodes, the electrolyte or the substrate. In order to investigate these different degradation mechanisms of the cell in more detail, impedance spectroscopy at different operating times was performed.

Figure 7 shows the corresponding Nyquist and Bode plots of the cell at OCV between 193 h and 1540 h. During this time the ohmic resistance in the high frequency range increased from about 260 mΩ cm^2 at 193 h to

Fig. 7 Impedance spectra of a MSC cell at OCV conditions during long-term electrolysis: Nyquist plot (top), Bode plot (bottom)
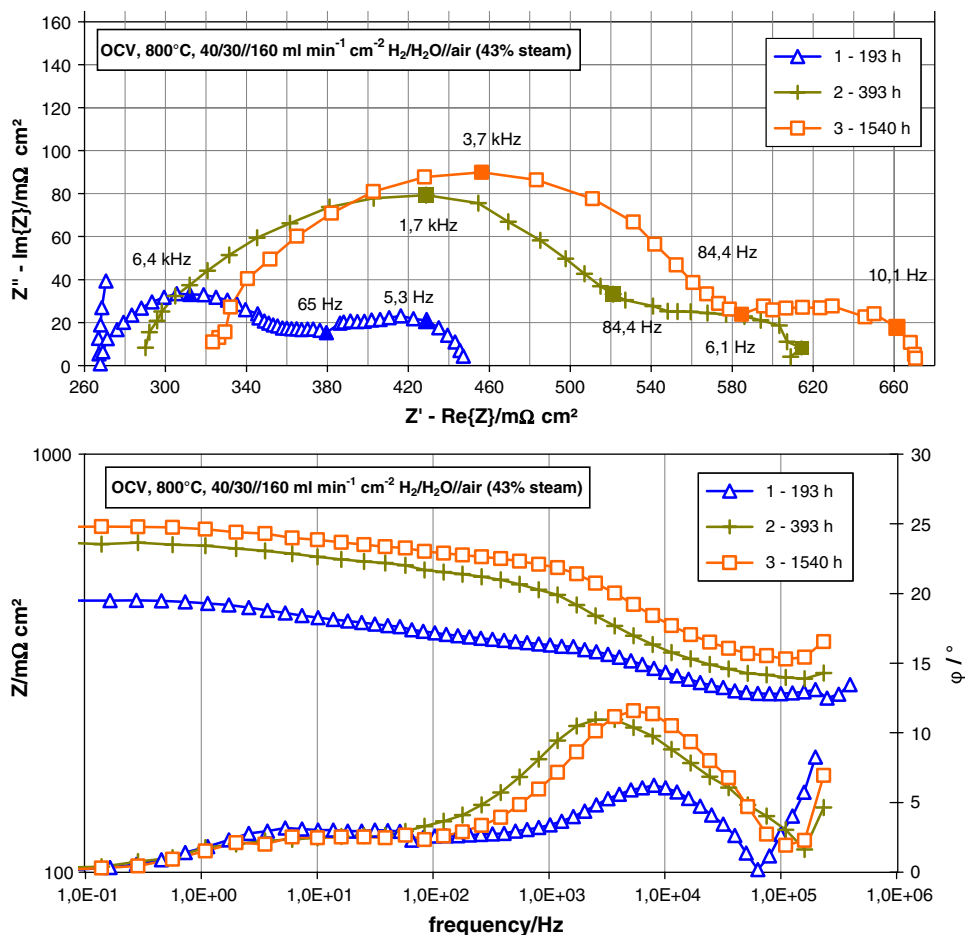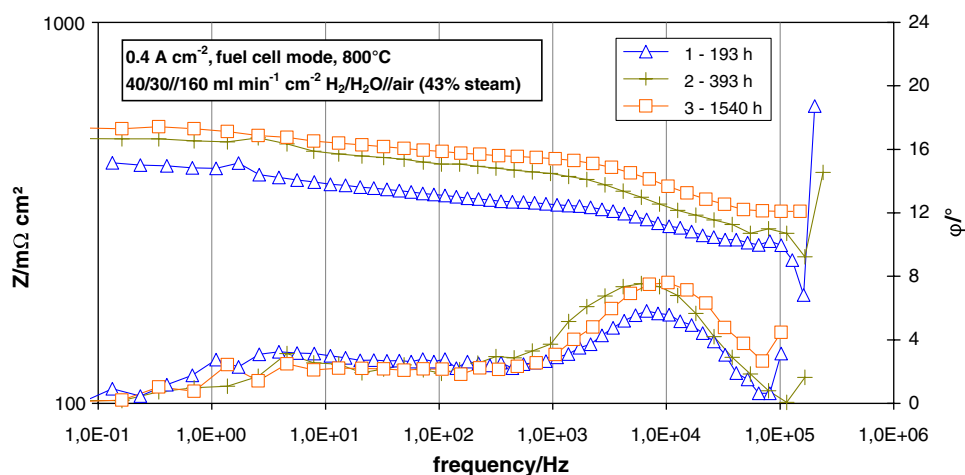

Fig. 8 Impedance spectra (Bode plot) of a MSC cell at 0.4 A cm^{-2} in fuel cell mode during long-term electrolysis

320 mΩ cm^2 at 1540 h. This increase of 60 mΩ cm^2 can be explained by oxidation processes of the porous metallic IT substrate which were observed in the microstructure of the substrate after the 2000 h of operation (see Fig. 10). Moreover, a significant increase of the overall impedance from 450 mΩ cm^2 to 670 mΩ cm^2 can be observed. This corresponds to an increase of the overall polarisation impedance from 190 mΩ cm^2 after 193 h to 320 mΩ cm^2

after 393 h and 350 mΩ cm^2 after 1540 h. The strongest change can be observed during the first 400 h when i-V characterisation measurements under temperature variation were performed, whereas after this period only relatively small changes were observed. The changes can be attributed to the increase of the polarisation resistances of the fuel and the O$_2$-electrode. Due to the strong overlapping of these two processes, it is difficult to clearly separate the

Fig. 9 Impedance spectra (Bode plot) of a MSC cell at -0.4 A cm^{-2} in electrolysis mode during long-term electrolysis: Nyquist plot (top), Bode plot (bottom)
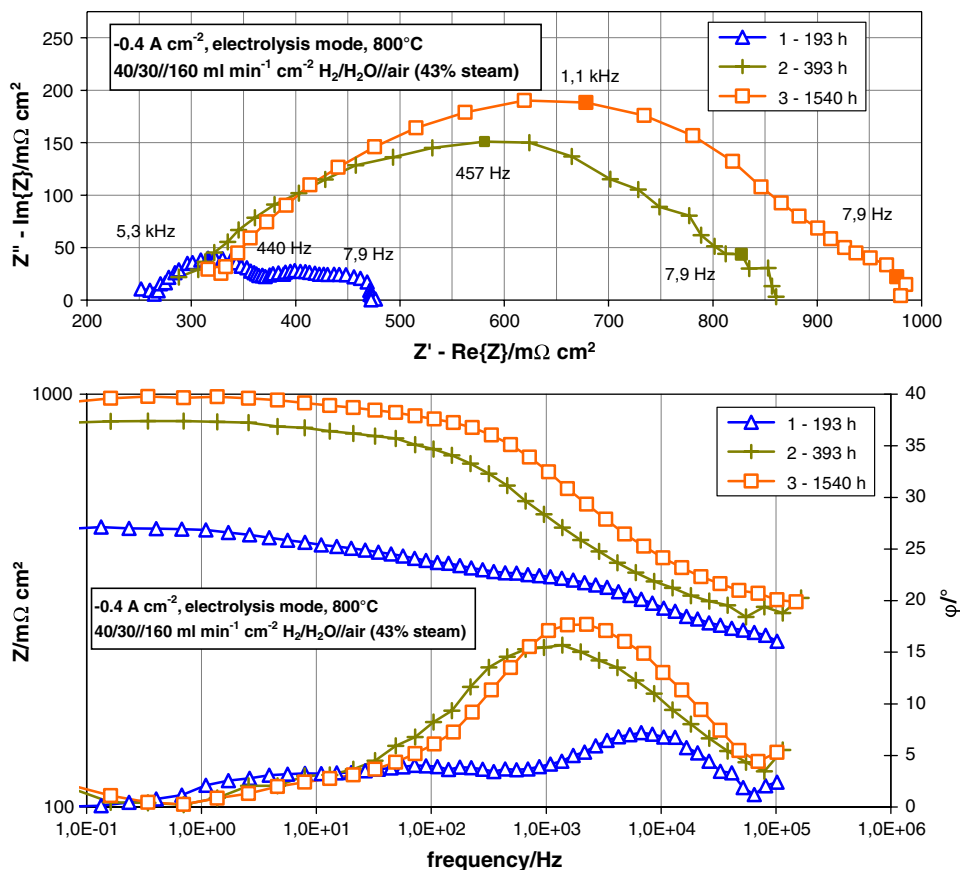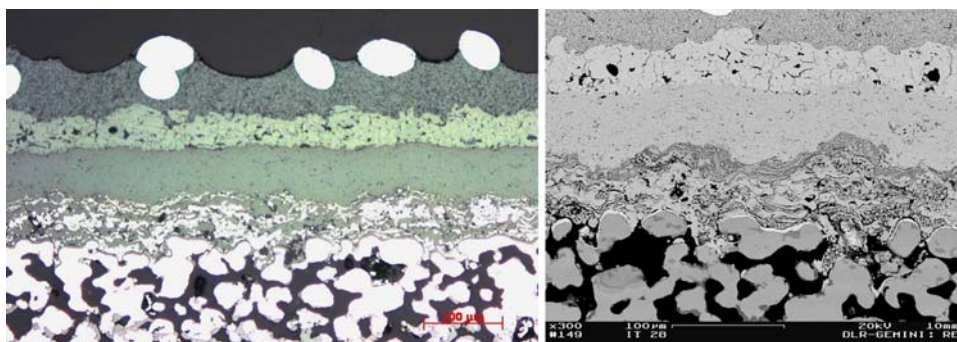

Fig. 10 Micrographs of the cross section of the plasma sprayed cell after 2425 h of operation (left: optical microscope/right: scanning electron microscope)

contribution of the hydrogen and oxygen electrode. However, the post-analysis of the microstructure of the cell after operation in Fig. 10 has shown coarsening especially of the Ni particles of the hydrogen electrode. This may lead to a decrease of the electrochemical activity of the hydrogen electrode through the reduction of the triple phase boundary.

In Figs. 8 and 9 the impedance spectra of the cell at a current density of 0.4 A cm^{-2} are shown in fuel cell and in electrolysis mode as a function of operating time. According to the theory, the ohmic resistances in fuel cell and electrolysis mode are identical. The values are in the range of 260–320 mΩ cm^2. Similar to the spectra at OCV in both cases an increase of the ohmic resistance of about 60 mΩ cm^2 during operation of 1540 h can be observed.

This increase can be explained with the above described formation of oxide layers in the porous metallic substrate. The overall impedances in the fuel cell mode are in the range of 170–220 mΩ cm^2 and are lower in comparison to the electrolysis mode. In this case the values are 220–660 mΩ cm^2. These differences can be explained by the higher polarisation resistances of the electrodes in the electrolysis mode. In this case, especially the high water content of the fuel electrode leads to a higher activation polarisation. Furthermore, the results of the impedance spectra are in good agreement with the slope of the current-voltage curves which represent the area specific resistances (ASR) of the cell. At a current density of 0.4 A cm^{-2} the slopes of the electrolysis curves are much higher in

Fig. 11 I-V and i-p characteristics of a single repeating unit (MSC cell with coated interconnect) during both fuel cell and electrolysis operation at 800 °C after different operating times (83 h and 290 h). Probes for voltage measurement are placed at the O$_2$-electrode (symbols x and †) and at the interconnect (symbols Δ and □). Gas flow: 40/30/160 mL min^{-1} cm^{-2} H$_2$/H$_2$O/air (43% steam)
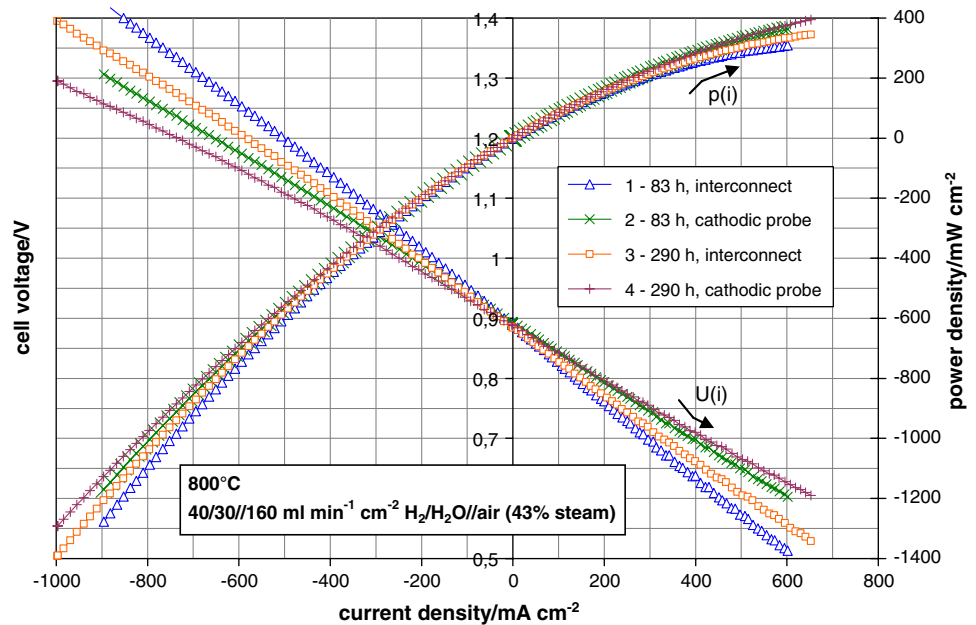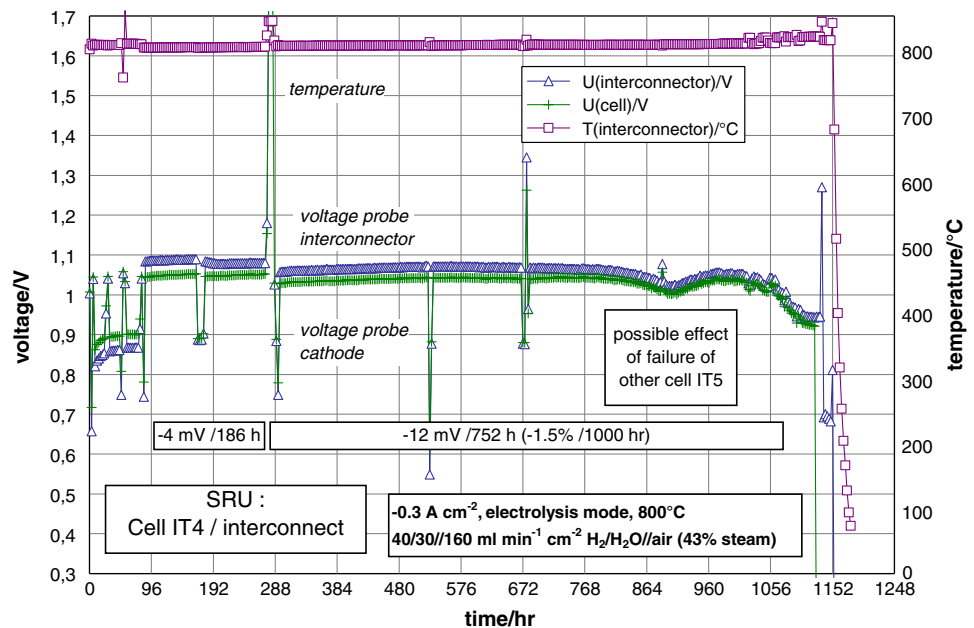

Fig. 12 Long-term test run of a single repeating unit (MSC cell with coated interconnect) with a continuous load of −0.3 A cm^{-2} in electrolysis mode over 940 h of operation; temperature (top) and voltage at different positions (at interconnect and at O$_2$-electrode) were monitored. Gas flow: 40/30/160 mL min^{-1} cm^{-2} H$_2$/H$_2$O/air (43% steam)

comparison to the slopes of the fuel cell curves. The increase of the overall polarisation impedances are therefore in the range of 440 mΩ cm^2 for the electrolysis mode and 50 mΩ cm^2 for the fuel cell mode. Hence, the degradation in polarisation resistance is much higher for electrolysis mode than for fuel cell mode. In both cases similar to the spectra at OCV, the strongest increase in polarisation resistances can be observed during the first 400 h.

A SEM micrograph of the cell after 2425 h of operation is shown in Fig. 10. Major changes in the different functional layers or cracks could not be observed. But oxide scales on the rim of the substrate particles indicate a certain

oxidation of the ferritic steel substrate during operation. EDX analysis (EDX mapping and EDX line-scan) of a cross section of the cell proved the efficiency of the PVD DBL. Only very small amounts of Fe and Cr species could be detected in the hydrogen electrode and no Ni species were found in the substrate indicating that species migration has been efficiently prevented by the DBL.

In addition to the single cell tests, test runs with SRU of a plasma sprayed cell and a metallic interconnect were performed. The cells were of the same type as described before including a DBL. Figure 11 showing the performance of an SRU in both fuel cell and electrolysis mode for different operating times (83 h and 290 h) reveals an

improvement of performance with time reaching a cell voltage of 1.3 V at -1.0 A cm^{-2} and 800 °C after nearly 300 h of operation when measured at the O$_2$-electrode. Voltage measurement at the interconnect showed a higher voltage of approximately 100 mV due to the contact resistance. Measurements with SRUs contacted without the Pt grid showed a much higher voltage indicating that the contacting area without the grid is much lower resulting in an enhanced contact resistance. To achieve good performance in a stack, contacting of cell and interconnect is a critical and important issue needing much attention to be paid.

The behaviour during long-term testing of the SRU is summarised in Fig. 12. At constant electrolysis operation with -0.3 A cm^{-2} over about 940 h practically no degradation was observed. In the period between 830 h and 960 h of operation the monitored cell voltage showed unusual behaviour with a decrease and a following increase which was probably caused by the failure of another SRU that occurred in that period in the same test rig.

References

1. Divisek J, Wendt H (1990) In: Wendt H (ed) Electrochemical hydrogen technologies. Elsevier, Amsterdam
2. Kreuter W, Hofmann H (1996) In: Veziroglu TN, Winter CJ, Baselt JP, Kreysa G (eds) Hydrogen energy progress XI. International Association for Hydrogen Energy, USA
3. Janssen H, Emonts B, Groehn HG, Mai H, Reichel R, Stolten D (2001) Hypothesis IV, Vol. 1:172
4. Schiller G, Henne R, Mohr P, Peinecke V (1998) Int J Hydrogen Energy 23(9):761
5. Mogensen M, Bagger C (1998) In: Proc. 1998 Fuel Cell Seminar Palm Springs CA (USA) 16–19 November 1998:96
6. Mogensen M, Jensen SH, Hauch A, Chorkendorff I, Jacobsen T (2006) In: Bossel U (ed) Proc. 7th European SOFC Forum Lucerne PO301
7. Dönitz W, Schmidberger R, Steinheil E, Streicher R (1980) Int J Hydrogen Energy 5(1):55
8. Dönitz W, Erdle E (1985) Int J Hydrogen Energy 10(5):291
9. Dönitz W, Erdle E (1990) In: Wendt H (ed) Electrochemical hydrogen energy technologies, electrochemical production and combustion of hydrogen. Elsevier, Amsterdam
10. Erdle E, Dönitz W, Schramm R, Kocha (1992) Int J Hydrogen Energy 17(10):817
11. Isenberg AO (1981) Solid State Ionics 3–4:431
12. Hartvigsen J, Elangovan S, O'Brien JE, Stoots CM, Herring JS, Lessing P (2004) In: Mogensen M (ed) Proc. 6th European SOFC Forum Lucerne :378
13. O'Brien JE, Stoots CM, Herring JS, Hartvigsen J (2006) J Fuel Cell Sci Tech 3(2):213
14. Hong HS, Chae U, Choo ST, Lee KS (2005) J of Power Sources 149:84
15. Wang WS, Huang YY, Jung SW, Vohs JM, Gorte RJ (2006) J of the Electrochem Soc 153(11):A2066
16. Uchida H, Osada NN, Watanabe M (2004) Solid-State Letters 7(12):A500
17. Osada NN, Uchida H, Watanabe M (2006) J of the Electrochem Soc 153(5):A816
18. Brisse A, Mogensen M, Schiller G, Vogt U, Zahid M (2008) In: Proc. 17th World Hydrogen Energy Conference (WHEC2008) Brisbane, Australia
19. Hauch A, Jensen SH, Mogensen M (2005) In: Solid State Electrochemistry—Proc. of the 26th Risø International Symposium on Material Science Roskilde Denmark:203
20. Hauch A, Jensen SH, Mogensen M, Ramousse S (2006) J Electrochem Soc 153(9):A1741
21. Hauch A, Jensen SH, Mogensen M, Bilde-Sørensen JB (2007) J Electrochem Soc 154(7):A619
22. Hauch A, Ebbesen SD, Jensen SH, Mogensen M (2007) In: Risø International Energy Conference Roskilde Denmark:327
23. Mogensen M, Jensen SH, Hauch A, Chorkendorff I, Jacobsen T (2007) In: Proc. 32nd International Cocoa Beach Conference on Advanced Ceramics and Composites, The American Ceramic Society
24. Henne RH, Franco T, Ruckdäschel R (2006) J Therm Spray Technol 15(4):695
25. Franco T, HoshiarDin Z, Szabo P, Lang M, Schiller G (2007) J Fuel Cell Sci Tech 4(4):406
26. Franco T, Schibinger K, Ilhan Z, Schiller G, Venskutonis A (2007) In: Proc. 10th International Symposium on Solid Oxide Fuel Cells (SOFC-X) Nara Japan 3–8 June 2007 electronic paper
27. Syed AA, Ilhan Z, Arnold J, Schiller G, Weckmann H (2006) J Therm Spray Technol 15(4):617
28. Ansar SA, Ilhan Z, Richter W (2007) High Temp Mater Process 11(1):83
29. Ansar SA, Ilhan Z (2007) In: MRS Spring Meeting San Francisco USA electronic paper